Research Article | Vol. 26, No. 22 | 29 Oct 2018 | OPTICS EXPRESS 28312
Optics EXPRESS

Pulse length variation causing spectral distortions in OPO-based hyperspectral coherent Raman scattering microscopy

CHRISTIAN PILGER, HENNING HACHMEISTER, PAUL GREIFE, ALEX WEIß, GERD WIEBUSCH, AND THOMAS HUSER*

Biomolecular Photonics, University of Bielefeld, Universitätsstr. 25, D-33501 Bielefeld, Germany
**thomas.huser@physik.uni-bielefeld.de*

Abstract: Picosecond optical parametric oscillators (OPOs) with broad wavelength tunability are frequently used as light sources in hyperspectral coherent Raman scattering (CRS) microscopy. We investigate how changes in the pulse length during OPO wavelength tuning of the pump beam affect hyperspectral CRS imaging. We find that significant distortions of the resulting CRS spectra occur if the OPO is operated without monitoring pulse length variations. By utilizing a custom-written MATLAB based control program to counteract changes in pulse length, normalized and reproducible data sets can be acquired. We demonstrate this by comparing hyperspectral data obtained from pure substances, as well as relevant biological specimens.

1. Introduction

In biomedical imaging coherent anti-Stokes Raman scattering (CARS) and stimulated Raman scattering (SRS) are well established microscopy methods, providing versatile and powerful label-free contrast mechanisms as compared to fluorescence imaging [1,2]. A wide array of applications have demonstrated the usefulness of probing and imaging specific molecular resonances related to a sample's chemical content [2]. More recently, this approach has been further extended in terms of specificity and sensitivity by tuning the probe wavelengths across a range of molecular resonances to capture a broader gamut of a sample's spectral information [3–12]. Hyperspectral CARS (HS-CARS) microscopy is just one implementation of this approach, which is independent of prior knowledge of the chemical content of the sample and can reveal additional spectral information [6].

The use of picosecond (ps) pulsed laser systems as light sources for HS-CARS typically requires the iterative tuning of the pump laser wavelength across the entire spectral range of interest while a series of images are acquired for each wavelength. The spectral information is then extracted by multivariate statistical analysis, by color coding or, highlighting special spectral aspects, by linear decomposition algorithms in post-processing [13–16]. In order to generate a reproducible spectrum of the specimen the laser intensity is usually measured and in a post-processing step the collected data is normalized [6]. The use of an OPO system necessitates such processing as intensity variations occur due to tuning the spectrally narrow pump beam.

Here, we investigate the effect of pulse length variations on HS-CARS data as a result of OPO tuning. A MATLAB based routine to control the OPO's performance in terms of selected wavelength, output power and pulse length was written as we show in Code 1 [17]. This software also controls the image scanning process and records the actual laser intensities used in the experiment via fast photodiodes enabling a subsequent post-processing step to normalize all HS-CARS image frames. We find that pulse length variations lead to significant distortions of the resulting spectral data, which can, however, be avoided by the corrections implemented through our custom-written control software.

Optics EXPRESS

2. Materials and methods

2.1 CARS imaging system

In this study a home-built CARS microscope is used for label-free imaging [18–21]. The main source is composed of a 7ps 1064nm Nd:VAN laser (picoTRAIN, High Q laser GmbH, Austria) operating at 80MHz repetition rate. The frequency-doubled 5.9ps 532nm beam pumps an optical parametric oscillator (OPO) (Levante Emerald, APE, Germany). The OPO delivers the tunable pump beam wavelengths for the CARS experiment while the 1064nm laser serves as non-tunable Stokes wavelength. After spatial and temporal overlapping of the two laser beams by a dichroic mirror and an optical delay stage the beams are coupled into a custom-built laser scanning microscope. Galvanometric scanning mirrors (Cambridge Technology, Galvanometer Optical Scanner, Model 6215H, USA) are utilized to raster scan the laser focus across the sample. A telescope fills the back focal plane of the 60x water immersion objective lens (Olympus UPlanSApo, NA = 1.2, Olympus, Germany) focusing the beams into the sample. The overall signal is collected in forward direction through a condenser lens (U-AAC, NA = 1.4, Olympus, Germany). The generated CARS signal is then isolated from the excitation laser wavelengths by a filter set composed of a 950 SP, a 785 SP, two 775 SP, and a 514 LP (all Semrock, USA) and is finally detected by a photomultiplier tube (PMT) (H 9656-20, Hamamatsu Photonics, Japan). The resulting electronic signal is acquired by an analog-to-digital (A/D) converter (PCI-6110S, National Instruments, USA) and analyzed by the MATLAB program ScanImage (version 3.8.1, Howard Hughes Janelia Farm Research Campus [22]).

2.2 Normalization and laser noise reduction during the CARS imaging process

Two pellicle beam splitters (Pellicle Beam splitter 8R/92T 25.4mm, Edmund Optics, USA) direct a small portion of the Stokes and the pump beam onto two photodiodes (PDB-C613-2, Luna Optoelectronics, USA), which record the intensities for every pixel. The electronic signals are acquired by an additional A/D converter (PCIe-6363, National Instruments, USA). In a post-processing step, this data is used to remove laser fluctuations of up to 100kHz from each image and also to normalize separate images to each other (Fig. 1(b)).

In order to perform this normalization step with the highest precision we characterized the wavelength-dependent transmission of the pellicle beam splitters and implemented it into our normalization algorithm as additional weight factors for each wavelength of the pump beam.

2.3 OPO wavelength tuning for hyperspectral CARS imaging

For hyperspectral image acquisition, the pump beam was tuned with a step size of 0.3nm before each image acquisition using a custom-written MATLAB routine which controls the OPO via a RS-232 interface and the scanning process of the microscope. The spectral tuning range of the pump beam usually spans from 800 to 830nm corresponding to a vibrational spectrum ranging from 2650 to 3100cm^{-1}.

In the OPO a lithium triborate crystal (LBO) is placed in a laser cavity and pumped by the 532nm laser beam. In order to generate the tunable signal and idler wavelengths the non-linear $\chi(2)$-process of parametric amplification is exploited. The temperature of the LBO crystal determines the phase-matching condition of the parametric amplification. Here, a typical spectral tuning range of 15nm around the center wavelength is obtained. Wavelength selection is performed by utilizing a tunable simplified Lyot filter scheme consisting of a polarizer and a single birefringent block which is placed inside the OPO's cavity. The Lyot filter further suppresses undesired wavelengths with each pass through the filter, resulting in a spectral width of approximately 0.3nm (full width at half maximum).

To optimize the OPO's signal wavelength power during wavelength tuning, both, the LBO crystal temperature T as well as the OPO's cavity length L_{cav} are altered simultaneously. L_{cav} is varied by a mirror mounted on a linear piezo translation stage. The control program

Optics EXPRESS

communicates with the OPO control unit changing the crystal temperature as well as the cavity length (see Fig. 1(a)). This keeps the pulse length constant while optimizing the output power and shifting the OPO wavelength. For this purpose the temperature response of the LBO crystal is characterized specifically in order to operate at the working point for each selected signal wavelength providing maximum intensity output. The temperature response curve is stored in the control program defining an optimal temperature t_{opt} for a certain signal wavelength and is unique to each system. In general the OPO works at the chosen signal wavelength in a temperature range of 3°C. Here, it changes the pulse length and output power in respect to the temperature. The cavity length is altered in an iterative process while optimizing the output power value provided by the OPO. The optimal cavity length is defined as L_{cav}^{Opt}. In general our custom-written OPO control software is independent of the use of an autocorrelator due to the correlation of maximum output power to longest pulse length.

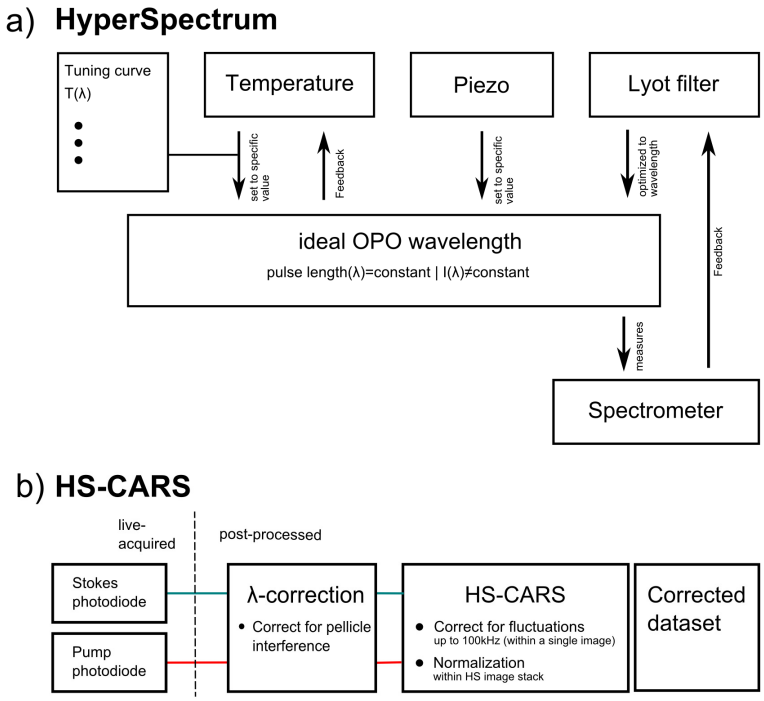

Fig. 1. (a) Block diagram of the custom-written MATLAB routine for dynamic OPO wavelength tuning enabling constant pulse length in hyperspectral CARS image acquisition. When the target pump wavelength is reached, the image acquisition starts automatically. The routine only grants constant pulse length, the output intensity for the selected wavelength can vary due to the OPO's crystal response. Therefore, the pump photodiode records the actual intensity applied to the sample. (b) shows the necessary post-processing steps, which uses simultaneously recorded photodiode data for removing intensity fluctuations from the laser sources up to 100kHz within a single image as well as to normalize the images of a hyperspectral scan between them.

2.4 Pulse length characterization during OPO wavelength tuning

An autocorrelator (pulseCheck 50, APE, Germany) is used to characterize the pulse length. The simultaneous measurement of the pulse length during each image acquisition is made possible by a pellicle beam splitter mounted in front of the microscope (Pellicle Beam splitter 8R/92T 25.4mm, Edmund Optics, USA). A custom-written MATLAB routine extracts the value of the pulse length from the manufacturer's software, assigning it to the images during

Optics EXPRESS

the hyperspectral CARS scan. Hence, the procedure and duration of the HS-CARS scan process are independent of the pulse length measurement. In Fig. 2 the schematic sequence of the hyperspectral CARS imaging experiments is visualized. For acquiring the spectral information we typically collect 47 images and assign the actual pulse length to every image. Due to the improved mechanical and thermal stability of our setup (sample drift less than 450nm over 75min in all dimensions), we were able to repeat the experiments on exactly the same location of the sample while changing the OPO working conditions, e.g. the crystal temperature, and thus the pulse length. Therefore, we can evaluate both approaches by comparing the spectra from a region of interest of the specimen.

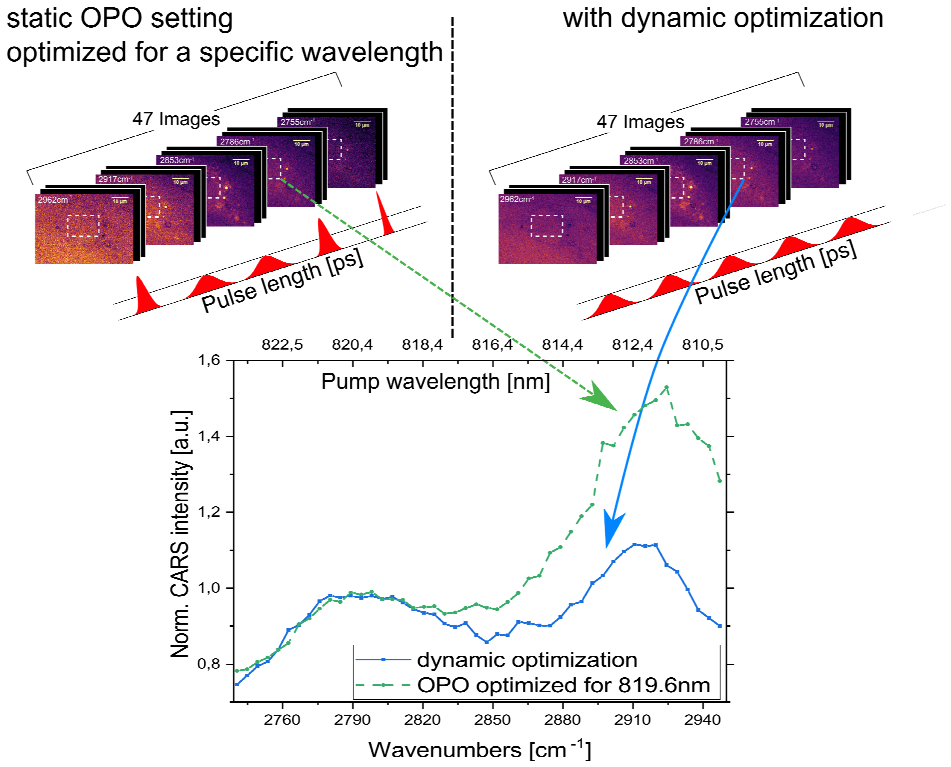

Fig. 2. Hyperspectral CARS image acquisition scheme. A series of CARS images is acquired while the pump wavelength delivered by the OPO is incrementally increased. Wavelength tuning of the OPO is controlled by a custom-written software routine, which adjusts the OPO parameters for the highest output power resulting in a mostly constant pulse length and stable operation. An autocorrelator is used to measure the pulse length of the pump beam after the optimization, the value of which is then assigned to every image. The blue spectrum (mean of all spectral measurements) is obtained by optimizing the OPO settings for constant pulse length and shows the data obtained in a region of interest representing a U2OS cell's nucleus. Repeating the experiment without the home-written program using a constant OPO setting instead results in the green spectrum.

2.5 Cell sample preparation

For biological experiments U2OS cells were grown on a large petri dish (50mm, No. 1.5, MatTek, USA) and fixed in place with 4% paraformaldehyde. In order to achieve the necessary focal and axial stability of the specimen, we dipped the condenser lens into the surrounding PBS-media of the cells. In addition, Immersol W 2010 (Carl Zeiss Jena GmbH, Germany) as immersion media was applied to the focusing water objective lens to avoid focal drifts due to the evaporation of the immersion media.

Optics EXPRESS

3. Results and discussion

In order to initially determine the influence of the OPO's tuning parameters on the pulse length of the pump beam in a CARS experiment, we investigated a pure dimethyl sulfoxide (DMSO) sample probing the CH/CD symmetric stretching mode at 2913cm^{-1}. We placed a drop of DMSO in a 'sandwich' between two coverslips (H878.2, Roth, Germany) separated by a 100µm thick Teflon ring. Using 12mW focal power of the 1064nm Stokes beam in combination with 23mW focal power of the wavelength-tuned pump beam, we integrated the resulting CARS signal over the full image (256x256px, 15.6µs per px) for each data point. Due to the varying output power of the OPO, we compensated the applied focal power before every measurement by a half-wave plate and a polarizing beam splitter cube (CM1-PBS252, Thorlabs, USA) using a power meter. The variation of the LBO crystal temperature T shows a variation of the pulse length from 3.6 to 5.4ps in a range of 3.5°C (Fig. 3(a)). The highest output power of the OPO, typically observed at t_{opt}, is determined corresponding to a pulse length of ~5.4ps. A non-linear dependence of the pulse length for t below (red crosses) or above (blue circles) t_{opt} is observed. The resulting CARS intensity occurring at 655.9nm is depicted in Fig. 3(b), where we normalized the data to the lowest CARS intensity at ~5.4ps pulse length. Here, we report an increase of the CARS signal by a factor of 1.51 due to the change in pulse length. A linear dependence of the CARS signal intensity on the pulse length can be observed in the data, which can be explained as follows: the intensity of the CARS signal scales quadratically with the pump beam intensity, which is comprised of the power and pulse length of the beam. While shortening the pulse length of the pump beam the temporal overlap with the Stokes beam, which has constant pulse length, is reduced leading to a decrease in CARS signal intensity. The decrease in this temporal overlap, which can be compared to "area matching" in temporal space, in combination with the quadratic increase of the CARS process, leads to the observed linear behavior.

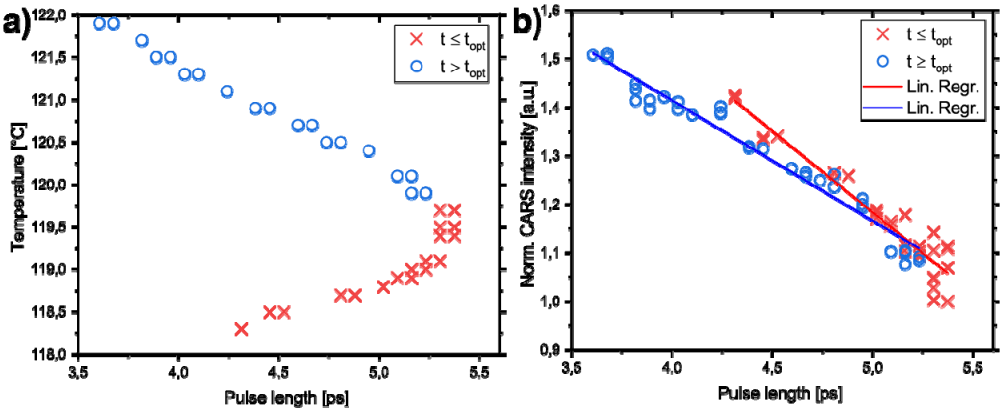

Fig. 3. Effect of the pulse length variation of the OPO output as a result of changes to the LBO crystal temperature measured by probing the CH/CD symmetric stretching resonance at 2913cm^{-1} in pure DMSO. (a) Tuning the LBO crystal temperature t in the OPO's cavity, while recording the pulse length of the pump beam results in pulse length variations in the range of ~5.4 to 3.6ps. t_{opt} is defined as the crystal temperature, which has the longest pulse length coinciding with the highest OPO signal output power. (b) The normalized CARS signal is plotted with respect to the pulse length. The red crosses indicate the crystal temperature below the optimal working point t_{opt} (at ~119.5°C as defined in (a)), the blue circles show the temperature above t_{opt}, respectively. The tuning range of the crystal temperature is ~3°C for the chosen pump wavelength. The cavity length of the OPO is kept constant. As can be seen, the CARS signal intensity is enhanced due to the decreasing pulse length by up to 51% compared to t_{opt}, which corresponds to ~5.3ps. A linear regression was included to guide the eye.

Optics EXPRESS

Holding the crystal temperature constant while tuning the cavity length of the OPO also leads to a change in pulse length compared to the optimal cavity length L_{cav}^{Opt} (see Fig. 4). L_{cav}^{Opt} describes the cavity length which generates the highest OPO output power and the longest pulse length. By detuning the cavity length the output pulses of the OPO are shortened while at the same time the output power decreases. Therefore, we readjusted the focal power at the sample before every measurement. In addition to that, while detuning the cavity, the optical path of the pump beam changes slightly (see Fig. 4(a)), which leads to a mismatch of the temporal overlap of the Stokes and pump beams in the CARS experiment. Hence, we also optimized the temporal overlap of the beams via the optical delay stage, resulting in a linear relationship of CARS signal intensity with respect to the pulse length (Fig. 4(b)). Compared to the optimal cavity setting the influence of this effect on the CARS signal was 71%. To clarify this behavior of the OPO we investigated, in a separate experiment, the repetition rate of the OPO by directing its signal output to a fast photodiode (DET10A, Thorlabs, USA). The photodiode's signal was analyzed with a spectrum analyzer (MDO 4054 B-6, 6GHz-spectrum analyzer function, Tektronix, USA) proving the repetition rate to remain constant while changing the cavity length in the range of 17-25.5µm (data not shown). In addition to that the temporal overlap of the Stokes and pump beams was analyzed using an oscilloscope (MSO 71254C, 100GS/s 12,5GHz, Tektronix, USA) in combination with a differential SMA probe (P7313SMA, Tektronix, USA) while using the laser's monitor photodiode signal as reference and trigger source. At a fixed position the pump beam was directed to the photodiode (DET10A) and then detected by the second channel of the oscilloscope, while comparing the 50% rising edge amplitude of both signals. Using the delay function of the oscilloscope the average of at least 35.45k triggered events was recorded for two settings of the OPO's cavity length. The data sets were finally subtracted from each other resulting in a change of the temporal overlap of 1.57 ± 0.52ps while shifting the OPO's cavity by 300digits (1digit ≈85nm).

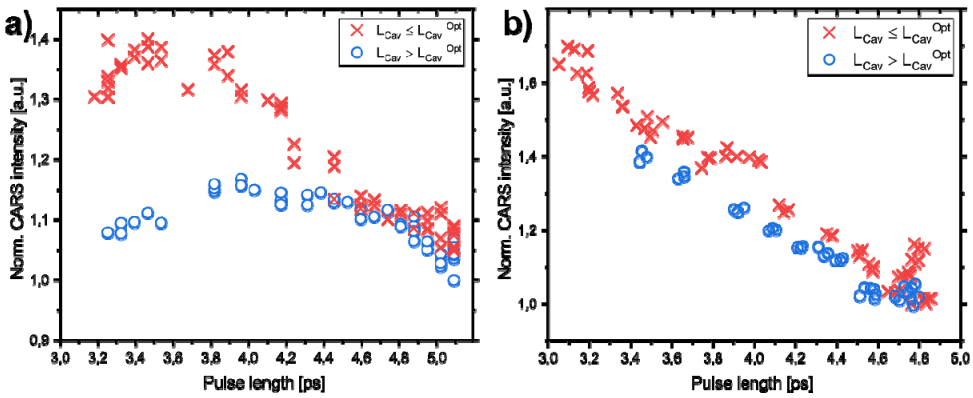

Fig. 4. Effect of the pulse length variation of the OPO output as a result of OPO cavity length detuning measured by probing the CH/CD stretching mode at 2913cm^{-1} in pure DMSO. a) Normalized CARS signal of DMSO with respect to the pulse length obtained during detuning of the cavity length of the OPO (changing the pulse length between ~5.1 to 3.2ps by shifting the cavity length in the order of 20µm). The signal wavelength as well as the crystal temperature is kept constant. Red crosses show a shorter cavity length than the optimal set point, blue circles show a longer cavity length. The optimal working point of the OPO is defined as the highest possible output power due to the chosen wavelength, coinciding with the longest pulse length. The measured CARS signal is different at the same pulse length (red and blue are not overlapping) and a nonlinear relation is observed. b) Normalized CARS signal obtained by continuously readjusting the temporal overlap. Due to the shorter pulse length resulting from cavity tuning, the CARS signal intensity varies by up to 71% with respect to the optimal set point at ~4.8ps.

Optics EXPRESS

Next, we investigated a full hyperspectral CARS image scan of pure methanol by probing the 2800 to 2955cm^{-1} region (corresponding to the pump wavelength range between 809nm to 818nm). Here, we altered the values of the OPO tuning parameters affecting the pulse length of the pump beam based on the previously conducted DMSO experiments. In Fig. 5(a) two resonances of the symmetric and anti-symmetric C-H stretching modes of methanol at 2830cm^{-1} and 2940cm^{-1} can be observed in the HS-CARS spectrum. The black curve shows the data that were acquired using the dynamic optimization of our custom-written control program, providing constant pulse duration. The blue curve shows the data acquired using a constant setting of the OPO parameters which were optimized for highest output power at 2800cm^{-1}. The red curve shows the same data where the OPO parameters were optimized for the 2870cm^{-1}, respectively. Note that all data sets were normalized to the 2823cm^{-1} peak to permit easy comparison. We observed a significant difference in the intensity of the second methanol resonance (2940cm^{-1}) between the blue curve and the black curve (constant pulse length) of up to 41%. Similarly, the red curve deviates from the black curve by up to 16%. To explain the origin of this discrepancy, Fig. 5(b) shows pulse length measurements corresponding to the HS-CARS spectra in Fig. 5(a). The black reference curve has a nearly constant pulse length of ~5ps, whereas the blue curve shows a strong decrease of the pulse length from the initial 5ps down to 3.6ps. A similar behavior can be seen in the red curve, where we observed a decrease in pulse length down to 4.0ps within the 8nm tuning range. Summarizing the effects observed with the methanol sample, we found that the OPO pulse length varies significantly depending on the wavelength and the initial OPO tuning parameters. If these parameters are not optimized throughout the OPO wavelength tuning process, the HS-CARS spectra will be distorted.

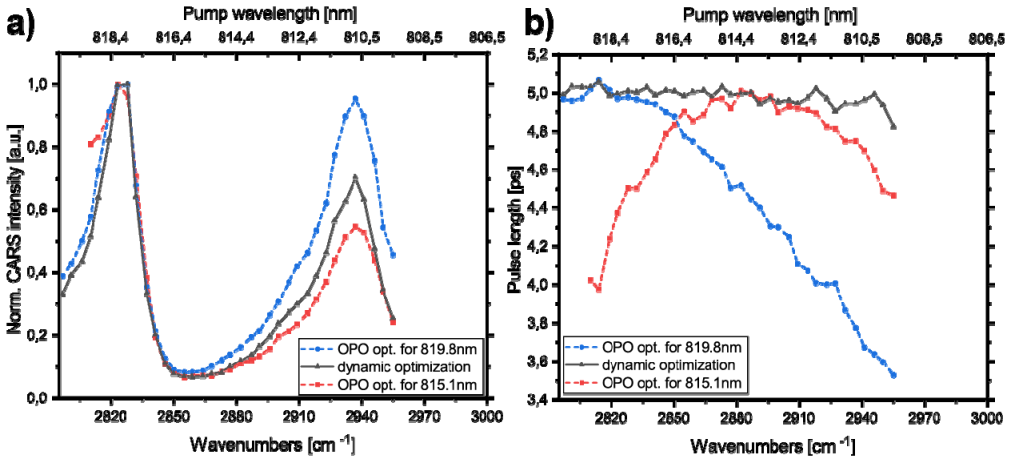

Fig. 5. Hyperspectral CARS spectroscopy of pure methanol. a) Normalized CARS intensity of pure methanol in the range of 2800cm^{-1} to 2955cm^{-1}. The two resonances at 2830cm^{-1} and 2940cm^{-1} of the symmetric and anti-symmetric C-H stretching mode are covered. CARS signal intensity is normalized to the peak at 2823cm^{-1}. The blue curve shows optimized settings of the OPO for best performance at 2800cm^{-1} (819.8nm), the red curve at 2870cm^{-1} (815.1nm), respectively. The black line depicts the result of dynamic optimization using our home-written program. b) Corresponding pulse length measured during wavenumber tuning. The custom-written MATLAB routine tunes the OPO while maintaining a constant pulse length (black curve). The blue curve shows the result of pulse length measurements with the OPO optimized for 2800cm^{-1} where the pulse length is longest (~5ps). The red curve shows the similar behavior with the optimum set at 2870cm^{-1}, respectively.

In order to investigate this effect for more complex samples we imaged fixed U2OS cells during a hyperspectral CARS scan consisting of 47 images with a spectral width of 4.7cm^{-1} ranging from 2738 – 2947cm^{-1}. We conducted the HS-CARS imaging process of these cells

Optics EXPRESS

three times for each of the previously discussed OPO settings (see the black curve in contrast to the blue and red curves obtained for methanol in Fig. 5). The repeat experiments verify that there is a minimal effect on the spectral response with time based on focal or lateral drifts. The duration of one hyperspectral scan was 27min, mostly determined by the waiting time for the temperature stabilization of the OPO's crystal. The following post-processing step took ~90s with a standard desktop personal computer. For the visualization of these HS-CARS image data we performed a principal component analysis (PCA) in MATLAB. All 47 images were subjected to the PCA analysis and the loadings for each pixel are color-coded in Fig. 6(a) [2,23].

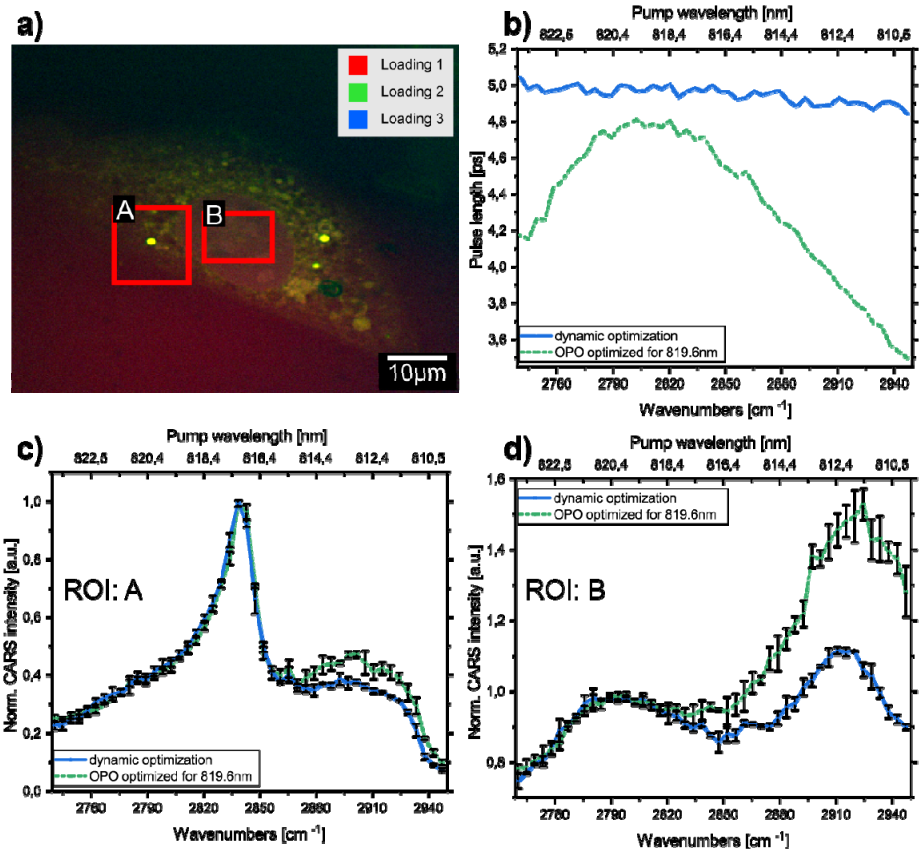

Fig. 6. HS-CARS imaging of a U2OS cell. a) HS-CARS image processed of a U2OS cell using principal component analysis (PCA) based on a hyperspectral image series. The spectral range from 2738 – 2947cm^{-1} was covered with a step size of ~4.5cm^{-1} while applying the dynamic OPO optimization. The duration of one hyperspectral scan was 27min, the following post-processing step took 90 seconds for the entire image stack. A total of 47 images were used for the PCA analysis. The image displays the color-coded loadings for each pixel. Two areas are chosen for further analysis containing the area of the cellular nucleus (ROI B) and a lipid droplet (ROI A). b) Pulse length variation during wavelength tuning. Dynamic optimization results in a constant pulse length of 4.9ps over the entire scan range (blue solid line). The static OPO setting (dashed green line) exhibits pulse length variations from 4.8ps at 819.6nm to 3.5ps at 810.0nm. Here, an initially optimized setting was found at 819.6nm and kept constant for the entire measurements of this experiment. c) Average HS-CARS spectra of all pixels from ROI A (a lipid droplet) and d) ROI B (the nucleus). Here, the spectra obtained using the dynamic optimization approach with constant pulse length are shown (blue solid line) in comparison to an OPO setting optimized for 2800cm^{-1} (dashed green line). The CARS signal intensity is normalized to the peak at 2840cm^{-1} for ROI A and 2780cm^{-1} for ROI B. Each scan was repeated three times with the standard deviation represented by the error bars.

Optics EXPRESS

Lipid droplets (Fig. 6(a), ROI A) as well as the nuclear region (Fig. 6(a), ROI B) of the U2OS cell are clearly discriminable. Hence, we compared spectra with constant pulse length (dynamic optimization) to non-constant pulse length for each ROI, respectively. The typical pump pulse length in these scans is 4.9ps for the entire scan range using the dynamic optimization mode, while the static OPO mode (initially optimized for 819.6nm) results in a varying pulse length depending on the pump wavelength, spanning from 4.8ps at 819.6nm to 3.5ps at 810.0nm (see Fig. 6(b)). The cell was scanned with both types of OPO control settings and we repeated each scan three times and calculated the average spectra (see Figs. 6(c) and 6(d)). The CARS signal intensities are normalized to the peak at 2840cm^{-1} for ROI A and 2780cm^{-1} for ROI B. The standard deviation of the single scans is shown as error bars. We observe low variance and high reproducibility of the spectra especially using the constant pulse length mode obtained by dynamic optimization (blue solid lines in Figs. 6(c) and 6(d)), while the green dashed line refers to constant OPO settings optimized at 819.6nm pump wavelength (2800cm^{-1}). As can be seen by comparing both spectra at the resonance at 2925cm^{-1}, the CARS intensity is up to ~50% higher for the static OPO setting (varying pulse length) as compared to the undistorted HS-CARS spectra obtained in dynamic optimization mode (see also Fig. 7).

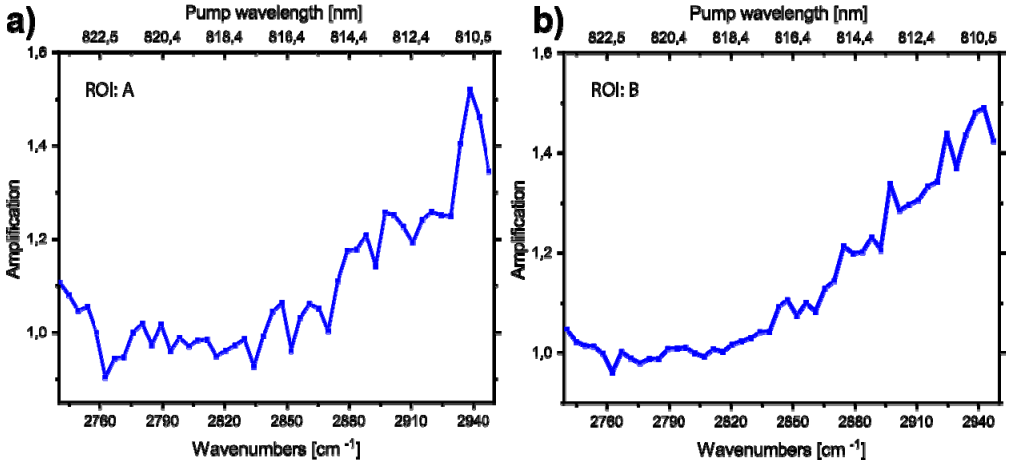

Fig. 7. Relative CARS signal variation during hyperspectral scanning due to pulse length variations. (a) Via dividing the green dashed curve (varying pulse length) by the solid blue curve (constant pulse length) of Fig. 5(a) (ROI A, lipid droplet) an enhancement of the spectral components at around 2940cm^{-1} (810.5nm pump) with a factor of 1.52 is observed. This is solely due to the variation of the pulse length during wavelength tuning. (b) The same operation performed for ROI B (nucleus). Here, a change in the relative CARS signal of up to 1.49 at 2940cm^{-1} (normalization to 2800cm^{-1}) is observed due to pulse length variations.

4. Conclusions

We investigated the influence of the pulse length of a picosecond OPO in a hyperspectral CARS experiment while changing the wavelength of the pump beam. Simultaneous measurements of the pulse length were performed by an autocorrelator. We found that both, the crystal temperature and the cavity length of the OPO result in changes of the output pulse length during automated wavelength tuning. This effect leads to significantly distorted HS-CARS spectra as demonstrated with pure DMSO and methanol. Analyzing HS-CARS images of a biological sample also demonstrated a strong signal dependence on the OPO pulse length. In order to avoid this effect we developed a custom-written MATLAB program that fully controls the OPO pulse length and keeps it constant during wavelength detuning. We provide this MATLAB code to anyone interested in using it for their own hyperspectral CARS experiments. In addition, this software also provides a noise suppression mode and the

Optics EXPRESS

normalization of the individual CARS images to each other in a hyperspectral series based on the total power deposited in the sample. The consequences of this work should also apply to hyperspectral stimulated Raman scattering when performed with an OPO system, due to the similar dependence of the SRS signal to potential variations of the pulse length during wavelength tuning.

Funding

Deutsche Forschungsgemeinschaft; Open Access Publication Fund of Bielefeld University.

Acknowledgments

We are grateful to Dr. Mathias Simonis for cultivating the U2OS cell samples. We thank Jens Hagemeyer, Dr. Mario Porrmann and Prof. Ulrich Rückert for the repeated loan of the high-speed digital oscilloscope. We acknowledge support for the Article Processing Charge by the Deutsche Forschungsgemeinschaft and the Open Access Publication Fund of Bielefeld University.

Disclosures

The authors declare no conflicts of interest related to this article.

References

1. J. X. Cheng and X. S. Xie, "Vibrational spectroscopic imaging of living systems: An emerging platform for biology and medicine," Science **350**(6264), 8870 (2015).
2. D. Zhang, P. Wang, M. N. Slipchenko, and J. X. Cheng, "Fast vibrational imaging of single cells and tissues by stimulated Raman scattering microscopy," Acc. Chem. Res. **47**(8), 2282–2290 (2014).
3. F. Hu, Z. Chen, L. Zhang, Y. Shen, L. Wei, and W. Min, "Vibrational imaging of glucose uptake activity in live cells and tissues by stimulated Raman scattering," Angew. Chem. Int. Ed. Engl. **54**(34), 9821–9825 (2015).
4. D. Fu, Y. Yu, A. Folick, E. Currie, R. V. Farese, Jr., T. H. Tsai, X. S. Xie, and M. C. Wang, "In vivo metabolic fingerprinting of neutral lipids with hyperspectral stimulated Raman scattering microscopy," J. Am. Chem. Soc. **136**(24), 8820–8828 (2014).
5. D. Zhang, P. Wang, M. N. Slipchenko, D. Ben-Amotz, A. M. Weiner, and J. X. Cheng, "Quantitative vibrational imaging by hyperspectral stimulated Raman scattering microscopy and multivariate curve resolution analysis," Anal. Chem. **85**(1), 98–106 (2013).
6. A. Fussell, E. Garbacik, H. Offerhaus, P. Kleinebudde, and C. Strachan, "In situ dissolution analysis using coherent anti-Stokes Raman scattering (CARS) and hyperspectral CARS microscopy," Eur. J. Pharm. Biopharm. **85**(3 3 Pt B), 1141–1147 (2013).
7. A. L. Fussell, P. Kleinebudde, J. Herek, C. J. Strachan, and H. L. Offerhaus, "Coherent anti-Stokes Raman scattering (CARS) microscopy visualizes pharmaceutical tablets during dissolution," Jove-J Vis Exp (2014).
8. B. Kann, H. L. Offerhaus, M. Windbergs, and C. Otto, "Raman microscopy for cellular investigations--From single cell imaging to drug carrier uptake visualization," Adv. Drug Deliv. Rev. **89**, 71–90 (2015).
9. F. Grasmeijer, A. L. Fussell, H. W. Frijlink, A. H. de Boer, and H. L. Offerhaus, "Chemical-selective imaging of adhesive mixtures for inhalation using coherent Anti-stokes Raman scattering (Cars) microscopy," J. Aerosol Med. Pulm. D **29**, A23 (2016).
10. B. Huang, S. Yan, L. Xiao, R. Ji, L. Yang, A. J. Miao, and P. Wang, "Label-free imaging of nanoparticle uptake competition in single cells by hyperspectral stimulated Raman scattering," Small **14**(10), 1703246 (2018).
11. R. He, Z. Liu, Y. Xu, W. Huang, H. Ma, and M. Ji, "Stimulated Raman scattering microscopy and spectroscopy with a rapid scanning optical delay line," Opt. Lett. **42**(4), 659–662 (2017).
12. L. Kong, M. Ji, G. R. Holtom, D. Fu, C. W. Freudiger, and X. S. Xie, "Multicolor stimulated Raman scattering microscopy with a rapidly tunable optical parametric oscillator," Opt. Lett. **38**(2), 145–147 (2013).
13. F. K. Lu, S. Basu, V. Igras, M. P. Hoang, M. B. Ji, D. Fu, G. R. Holtom, V. Neel, C. W. Freudiger, D. E. Fisher, and X. S. Xie, "Label-free DNA imaging in vivo with stimulated Raman scattering microscopy (vol 112, pg 11624, 2015)," Proc. Natl. Acad. Sci. U.S.A. **112**(37), E5902 (2015).
14. M. Miljković, T. Chernenko, M. J. Romeo, B. Bird, C. Matthäus, and M. Diem, "Label-free imaging of human cells: algorithms for image reconstruction of Raman hyperspectral datasets," Analyst (Lond.) **135**(8), 2002–2013 (2010).
15. B. M. Davis, A. J. Hemphill, D. C. Maltaş, M. A. Zipper, P. Wang, and D. Ben-Amotz, "Multivariate hyperspectral Raman imaging using compressive detection," Anal. Chem. **83**(13), 5086–5092 (2011).
16. N. Bergner, A. Medyukhina, K. D. Geiger, M. Kirsch, G. Schackert, C. Krafft, and J. Popp, "Hyperspectral unmixing of Raman micro-images for assessment of morphological and chemical parameters in non-dried brain tumor specimens," Anal. Bioanal. Chem. **405**(27), 8719–8728 (2013).
17. C. Pilger, figshare (2018) [retrieved 22 August 2018], https://doi.org/10.6084/m9.figshare.6993644.v1.

Optics EXPRESS

18. T. Weeks, S. Wachsmann-Hogiu, and T. Huser, "Raman microscopy based on doubly-resonant four-wave mixing (DR-FWM)," Opt. Express **17**(19), 17044–17051 (2009).
19. I. W. Schie, J. Wu, T. Weeks, M. A. Zern, J. C. Rutledge, and T. Huser, "Label-free imaging and analysis of the effects of lipolysis products on primary hepatocytes," J. Biophotonics **4**(6), 425–434 (2011).
20. A. D. Hofemeier, H. Hachmeister, C. Pilger, M. Schurmann, J. F. W. Greiner, L. Nolte, H. Sudhoff, C. Kaltschmidt, T. Huser, and B. Kaltschmidt, "Label-free nonlinear optical microscopy detects early markers for osteogenic differentiation of human stem cells," Sci. Rep. **6**, 26715 (2016).
21. D. Jaeger, C. Pilger, H. Hachmeister, E. Oberlander, R. Wordenweber, J. Wichmann, J. H. Mussgnug, T. Huser, and O. Kruse, "Label-free in vivo analysis of intracellular lipid droplets in the oleaginous microalga Monoraphidium neglectum by coherent Raman scattering microscopy," Sci. Rep. **6**, 35340 (2016).
22. T. A. Pologruto, B. L. Sabatini, and K. Svoboda, "ScanImage: flexible software for operating laser scanning microscopes," Biomed. Eng. Online **2**(1), 13 (2003).
23. I. W. Schie and T. Huser, "Methods and applications of Raman microspectroscopy to single-cell analysis," Appl. Spectrosc. **67**(8), 813–828 (2013).